INSTITUTE OF PHYSICS PUBLISHING PLASMA PHYSICS AND CONTROLLED FUSION

Plasma Phys. Control. Fusion **48** (2006) 1347–1372 doi:10.1088/0741-3335/48/9/006

Weak effect of ion cyclotron acceleration on rapidly chirping beam-driven instabilities in the National Spherical Torus Experiment

W W Heidbrink[1], E Ruskov[1], E D Fredrickson[2], N Gorelenkov[2], S S Medley[2], H L Berk[3] and R W Harvey[4]

[1] University of California, Irvine, California, USA
[2] Princeton Plasma Physics Laboratory, Princeton, New Jersey, USA
[3] University of Texas, Austin, Texas, USA
[4] CompX, Del Mar, California, USA

Received 5 March 2006, in final form 13 July 2006
Published 3 August 2006
Online at stacks.iop.org/PPCF/48/1347

Abstract

The fast-ion distribution function in the National Spherical Torus Experiment is modified from shot to shot while keeping the total injected power at ∼2 MW. Deuterium beams of different energy and tangency radius are injected into helium L-mode plasmas, producing a rich set of instabilities, including compressional Alfvén eigenmodes, toroidicity-induced Alfvén eigenmodes (TAE), 50–100 kHz instabilities with rapid frequency sweeps or chirps, and strong, low frequency (10–20 kHz) fishbones. The experiment was motivated by a theory that attributes frequency chirping to the formation of holes and clumps in phase-space. In the theory, increasing the effective collision frequency of the fast ions that drive the instability can suppress frequency chirping. In the experiment, high-power ($\lesssim$3 MW) high harmonic fast wave (HHFW) heating accelerates the fast ions in an attempt to alter the nonlinear dynamics. Steady-frequency TAE modes diminish during the HHFW heating but there is little evidence that frequency chirping is suppressed.

(Some figures in this article are in colour only in the electronic version)

1. Introduction

Instabilities that are driven by the fast-ion population have been extensively studied in toroidal devices for decades [1]. An understanding of the nonlinear dynamics of these instabilities is essential to predict the amplitude and subsequent fast-ion transport associated with alpha-driven instabilities in the International Thermonuclear Engineering Reactor (ITER) and other burning plasmas. The frequencies of fast-ion driven instabilities often sweep upward or downward in time. Frequency sweeping can arise in several ways. First, if the instability is a normal mode of the background plasma, the frequency changes as plasma parameters evolve; this

frequency sweeping occurs on a relatively slow 10–100 ms timescale and is explicable in terms of linear theory. For example, early measurements of the toroidicity-induced Alfvén eigenmode (TAE) noted that the mode frequency varies with the Alfvén speed when the plasma density changes [2, 3]. Frequency sweeping of normal modes can also occur nonlinearly as resonant fast ions respond to the wave; these changes can occur on a shorter (sub-millisecond) timescale. In addition to the excitation of normal modes of the background plasma, some instabilities are energetic particle modes (EPM) [4], which are distinct wave branches that require a fast-ion population to exist. The frequencies of these waves can also evolve rapidly if the fast-ion population that determines the wave's dispersion relation is altered by the growing wave. A familiar example of an EPM with rapid frequency sweeping is the classic fishbone [5]; the frequencies of these modes drop by a factor of two in less than a millisecond. In this paper, frequency 'chirping' refers to large changes in frequency on a sub-millisecond timescale.

The phenomenon of rapid chirping driven by energetic particles is extremely common. It occurs for classic fishbones [5] in many different conventional tokamaks [1]. Chirping in the frequency band between the TAE and classic fishbones was first observed during beam injection into the DIII-D tokamak [6] and was subsequently found in nearly all toroidal devices with intense beam injection including spherical tokamaks [7], conventional tokamaks (called 'bursting modes' in [8, 9]), and helical devices [10, 11]. Fast-ion populations created by intense ion-cyclotron heating can also excite rapid chirping [12, 13]. Qualitatively similar phenomena are driven by intense fast-electron populations in conventional tokamaks [14–16] and in a dipole experiment [17, 18]. The widespread nature of the phenomenon in systems with different instabilities and different energetic particle populations suggests that a generic theoretical model of the coupled wave-particle system might describe the essential features.

Berk, Breizman, and collaborators have attempted to develop such a model. They explore a simplified system: the classic 'bump-on-tail' Bernstein–Greene–Kruskal (BGK) [19] problem of a distribution function that excites electrostatic waves. The basic idea is that the velocity–space gradient that drives the instability is analogous to a phase-space gradient that drives fast-ion instabilities. For example, distorting the velocity distribution function in the bump-on-tail electrostatic problem is analogous to distorting the spatial gradient of resonant fast ions in an Alfvén wave problem. Berk *et al* find that, independent of the particular physical system, four characteristic frequencies determine the nonlinear dynamics of the resonant particles [20, 21]. Instability occurs when the linear growth rate γ_L of the kinetic drive exceeds the damping of the background plasma γ_d. The subsequent evolution depends on the characteristic bounce frequency of the resonant particles that are trapped in the finite amplitude wave ω_b compared with the rate ν_{eff} that particles leave and enter the resonance region in phase-space due to collisions (or other stochastic processes). In their model [22], frequency chirping is associated with the formation of holes and clumps in phase-space that describes the fast-particle distribution function. When collisions are weak, these phase-space structures persist and frequency chirping is possible. When the effective collision rate is large, the structures are rapidly destroyed and no frequency chirping occurs [23]. In the weakest collisional regime, the Berk–Breizman (BB) hole–clump model applies to a single normal mode. An explosive precursor occurs [21] that evolves into the formation of a hole and clump in phase-space [24]; the wave frequency locks onto the linear resonance frequency of the resonant particles. Next, the dissipation that is present in the background plasma forces the wave-trapped resonant particles to move in phase-space in such a way that the excited waves release energy while still nearly maintaining the wave amplitude. For the bump-on-tail problem and the Alfvén wave problem, this causes an increase in the hole resonant frequency while causing a decrease in the clump resonant frequency. In other physical situations, such as when resonant particles respond with an effective negative mass, it is possible for holes to decrease

and clumps to increase in frequency. With various weak perturbation assumptions, including that the gradient of the equilibrium phase-space distribution does not change appreciably as the phase-space structures move in phase-space, the BB hole–clump model predicts that the frequency chirp $\delta\omega$ tracks the phase-space perturbation, with a time evolution

$$\delta\omega \propto \sqrt{\delta t}. \tag{1}$$

Many features of the BB model are qualitatively consistent with experimental observations. A semi-empirical predator–prey model where the mode amplitude 'preys' on the fast-ion population accounts for many features of the cycle of instability bursts and particle losses that are often observed [25]; the possibility of repetitive burst cycles is a natural consequence of the BB model when beam fueling is included [26]. Tokamak fusion test reactor (TFTR) observations of the saturated amplitude near the linear stability threshold, of multiple modes well above threshold, of predator–prey burst cycles during neutral-beam injection, and of changes in mode amplitude when the ion cyclotron heating power is turned off can all be explained in terms of changes in γ_L, γ_d, ω_b, and ν_{eff} [27, 28]. Observations on the Joint European Torus (JET) that a single-frequency mode can split into multiple lines [29] or even become chaotic [30] as the fast-ion drive increases are consistent with the BB model. The time evolution of a frequency chirping TAE mode in the mega-ampere spherical tokamak (MAST) agrees well with modelling based on BB theory in agreement with equation (1) [31]; also, the repetitive cycle of chirping bursts is reproduced by the model [32]. Modes in MAST that chirp upwards in frequency, downwards, or in both directions can also be explained [33], as can upward frequency chirping of geodesic acoustic modes in JET [34]. A detailed test of the BB model was performed in a dipole experiment [17, 18]. A population of energetic electrons drove a strongly chirping interchange instablity. When electron cyclotron heating was added to increase the effective collision frequency of the resonant electrons, chirping was suppressed. (Note that, in this generalized definition, ν_{eff} is any stochastic process that scatters the particles out of resonance, not necessarily the collision rate that shapes the distribution function.) Quantitative estimates of γ_L, γ_d, ω_b, and ν_{eff} explained the observations.

In the theory of fast-ion driven instabilities, a distinction is made between perturbative and non-perturbative calculations. In a perturbative calculation, the spatial structure of the mode is barely altered by the fast-ion population; in other words, the linear eigenfunction is assumed constant throughout the calculation. In this sense, the BB hole–clump theory that predicts equation (1) is a perturbative theory because the gradient of the distribution function that models the fast-ion spatial gradient barely changes in response to the instability. The starting frequency of each chirping burst is the frequency of the underlying linear normal mode. When the system is strongly driven, several assumptions of the perturbative BB model can fail. For example, the population of resonant particles can cause a significant frequency shift in linear theory, the frequency shift of the chirp may cause the gradient of the resonant particles to change significantly during the chirp, and secondary phase-space instabilities may arise. Detailed numerical simulation of the bump-on-tail instability [35] shows that there are regimes where the frequency chirping becomes nearly linear in time, i.e.

$$\delta\omega \propto \delta t. \tag{2}$$

Nevertheless, as in the perturbative BB model, hole–clump phase-space structures together with the background dissipation are still responsible for frequency sweeping. Sophisticated calculations of the magneto-hydrodynamic (MHD) equations with kinetic wave-particle resonances have also simulated the frequency chirping phenomenon caused by the formation of phase-space structures [36–38].

Frequency chirping can also arise in more complicated non-perturbative models. Instability in the presence of multiple modes can cause an 'avalanche' in space that causes

frequency sweeping [26]. Consider a plasma with many weakly damped modes that have different spatial eigenfunctions. When the fast-ion gradient exceeds the linear threshold for one of the modes, spatial transport occurs, which increases the fast-ion gradient at a new location, destabilizing another mode. Transport by this mode moves the fast ions further, which steepens the gradient at a new location, destabilizing another mode, and so on. Rapid motion of the radial mode structure can also occur for an EPM with a single toroidal mode number [39]. In this case, the EPM radial envelope propagates radially due to the radial dispersiveness of the mode (a property of the linear dispersion relation) and because of the rapid redistribution of the energetic particle source (a manifestation of the nonlinear EPM group velocity). This phenomenon is particularly likely when the poloidal wavelength is short relative to the fast-ion pressure gradient scale length (i.e. $nq \gg 1$) but can also occur for $nq \gtrsim 1$. (n is the toroidal mode number and q is the safety factor.) Simulations show that the mode frequency chirps as the fast-ion gradient shifts outward in response to the instabilities [39]. In contrast to the BB model, this mechanism does not require fine structures in phase-space to generate frequency chirping.

The National Spherical Torus Experiment (NSTX) is an excellent testbed for the study of frequency chirping fast-ion instabilities. Many different fast-ion instabilities are observed during neutral beam injection [40]. One class of chirping instabilities [41] resemble the classic fishbone [5]: the toroidal mode number n is unity, the frequencies sweep downwards between 10–20 kHz, and the modes occur when $q_0 < 1$. (q_0 is the central safety factor.) A second class of chirping instabilities have frequencies that rapidly sweep through the TAE band (50–100 kHz) and can have a variety of toroidal mode numbers from $n = 1$ to above $n = 5$. There are also instabilities with steady frequencies in the TAE frequency band [41,42]. Another class of chirping instabilities are $n = 1$ modes with frequencies of $\sim$100 kHz and $\lesssim$ 20% frequency sweeps; these modes occur during the current ramp in virtually all beam-heated NSTX discharges. Finally, instabilities in the MHz range that are compressional Alfvén eigenmodes (CAE) [43,44] and global Alfvén eigenmodes (GAE) [40,44] also occur in most beam-heated NSTX discharges. These modes usually have steady frequencies but sometimes frequency chirping occurs in this frequency band as well [45]. To date, there is no definitive evidence of fast-ion losses during CAE activity [46] but the lower frequency modes all cause measurable losses under certain conditions [41].

The experiment reported here is motivated by the dipole experiment that used cyclotron heating to suppress frequency chirping [17, 18]. The basic idea of the experiment is to use neutral beam injection to create chirping instabilities, then use high harmonic fast wave (HHFW) heating to scatter the fast ions that drive the instabilities out of resonance, thereby suppressing the frequency chirping. The results of the experiment were unexpected: HHFW has no effect on the fishbone and TAE chirping instabilities but does alter the steady-frequency TAEs. The plasma conditions and fast-ion distribution functions are described in section 2. Section 3 summarizes the effect of changes in the distribution function on the various fast-ion instabilities. Possible explanations for the experimental observations are discussed in section 4, followed by the conclusions in section 5.

2. Experimental conditions

2.1. Plasma conditions

The data are from one day of NSTX [47] operation in 2004. The experiment consists of injecting various neutral beams with and without HHFW heating into nominally identical discharges to study the effect of the fast-ion distribution function on the instabilities. A typical discharge is shown in figure 1. All shots are heated with 2 MW of deuterium beams, the flattop

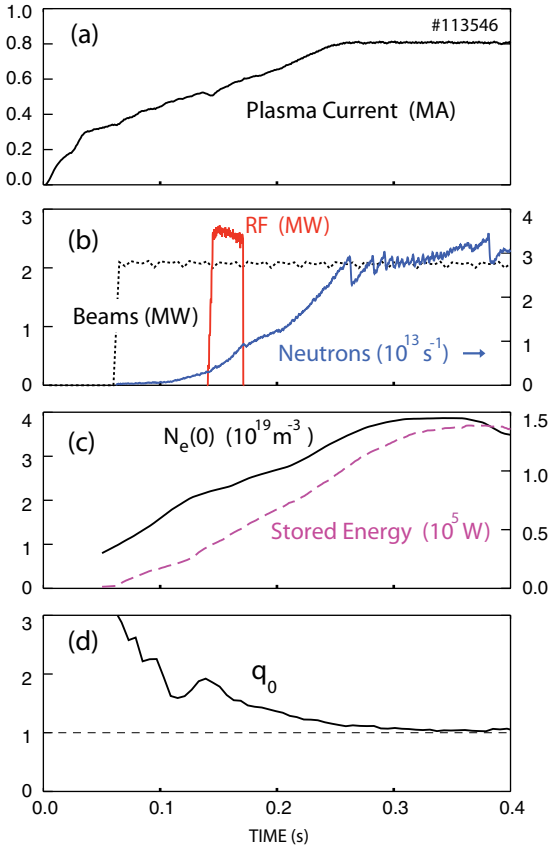

Figure 1. Time evolution of (*a*) the plasma current, (*b*) the neutral beam power (dashed line), RF power, and the neutron emission, (*c*) the central electron density (solid) and stored energy (dashed) calculated by the TRANSP code and (*d*) central q-profile calculated by the EFIT code in a typical discharge.

plasma current is 800 kA, and the vacuum magnetic field on axis is 0.4 Tesla. HHFW heating is applied at different times in the discharges, typically for 30 ms, and at a $\gtrsim$2 MW level. The electron density generally rises and q_0 generally falls as the discharge evolves. Reproducible L-mode plasmas are obtained by limiting the plasma on the graphite inner wall and by using helium as the working gas. Deuterium from the walls and from beam fueling also contributes to the ionic composition of the plasma. Typical plasma profiles are shown in figure 2. The electron temperature and density are measured by Thomson scattering [48]; the peak central temperature is $\sim$1.7 keV and the peak central density is $\sim 4 \times 10^{13}$ cm^{-3} (figure 2(*a*) and (*b*)). Because the electron density is relatively low, the beam density profile computed by the TRANSP code [49] peaks strongly on axis (figure 2(*c*)). The q profile (figure 2(*d*)) and other equilibrium parameters (figure 3(*a*)) are determined from EFIT reconstructions [50] using external magnetics measurements and the assumption that $q_0 = 1$ when sawteeth begin.

2.2. Neutral beam distributions

Variation in the beam distribution function is achieved by changing the angles and energy of beam injection. NSTX is equipped with three neutral beam sources that inject at tangency

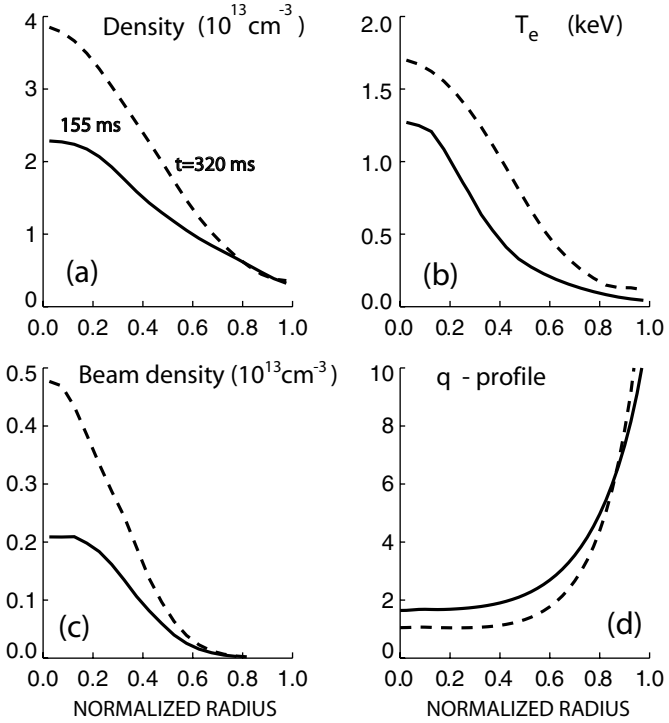

Figure 2. Plasma profiles versus normalized minor radius early (155 ms) and late (320 ms) in the discharge shown in figure 1. (*a*) electron density (*b*) electron temperature (*c*) beam-ion density assuming neoclassical fast-ion confinement and (*d*) q-profile as calculated by EFIT from external magnetics measurements.

radii of $R_{\rm tan} = 0.69$ m (source A), 0.59 m (source B), and 0.49 m (source C) (figure 3(*b*)). A single source at $E_{\rm inj} = 90$ keV or a pair of sources at 65 keV each inject $\sim$2 MW of power. Five conditions are studied: sources A, B, and C individually at 90 keV and sources A & B and sources B & C at 65 keV. Because the beam power is nearly identical and the plasma conditions are carefully selected, the neutral beam variations only result in slight variations of the electron temperature ($\lesssim 15\%$) and density ($\lesssim 10\%$) throughout the entire sequence. For all beam combinations, the maximum of the fast-ion pressure gradient occurs near a normalized minor radius of 0.3.

NSTX is a low-field, high-beta device. The fast ions have large gyroradii and large orbit shifts (figure 3(*a*)). The majority of the fast ions have speeds that exceed the Alfvén speed. The relatively low electron temperature implies that, classically, beam ions slow down primarily on thermal electrons. Accordingly, the classical pitch-angle scattering rate is an order of magnitude smaller than the energy deceleration rate. Under these conditions, the ion temperature, plasma rotation, and $Z_{\rm eff}$ profile (which are unavailable for most of the discharges) have little effect on the classical beam ion confinement and the fast-ion pitch angle is determined primarily by the angle of beam injection. Calculations of the classically-expected fast-ion distribution function are shown in figure 4. The steps in the distribution function associated with injection of half- and third-energy neutrals is evident in figure 4(*a*). Figures 4(*b*)–(*f*) shows that the variations in injection angle and energy substantially alter the fast-ion distribution function. The illustrated distributions are for a particular time (170 ms)

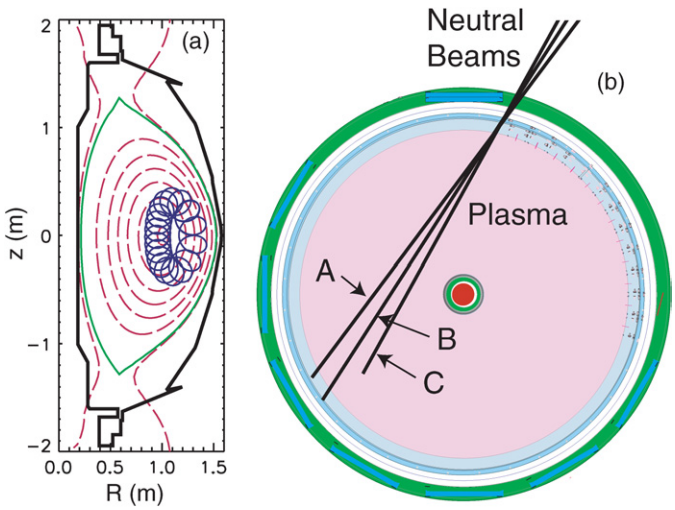

Figure 3. (*a*) Elevation of NSTX showing the vacuum vessel (thick line), the projection of an orbit of a 90 keV deuterium ion that is born near $R = 1.3$ m with $v_\parallel/v \simeq 0.41$, and some flux surfaces (dashed lines) for one of the experimental equilibria (discharge #113546 at 300 ms). The equilibrium parameters are: major radius of magnetic axis $R_0 = 1.01$ m; minor radius $a = 0.66$; toroidal field on axis $B_0 = 0.44$ T; elongation $\kappa = 1.9$; triangularity $\delta = 0.44$; toroidal beta $\beta_T = 9.6\%$; safety factor at surface that encloses 95% of the poloidal flux $q_{95} = 6.8$. (*b*) Plan view of NSTX showing the angles of injection of the three neutral beam sources.

early in the discharge. The five distributions retain these features later in the discharge, except that the rising electron temperature broadens the distributions in pitch angle as Coulomb scattering on thermal ions increases in importance.

2.3. Effect of HHFW on the fast-ion distribution function

HHFW is applied at two different times in the discharge. The 30 MHz fast waves are launched with a parallel wave number of $k_\parallel = 14\ \mathrm{m}^{-1}$, the value of $k_\parallel$ that maximized fast-ion absorption in previous experiments [51]. A relatively small outer gap of 3–4 cm is employed for efficient wave coupling in these L-mode plasmas. Although some edge ion heating can occur through parametric decay [52], the bulk of the power is absorbed by fast ions under these conditions. For classification purposes, we refer to the two HHFW times as 'early' and 'late.' The early HHFW is applied at ∼150 ms when the plasma current is still ramping up (figure 1(*b*)); the late HHFW is applied at ∼300 ms when the 800 kA steady-state current is already reached and q_0 approaches unity.

The application of HHFW gives perpendicular energy to the fast ions. Energy spectra measured by a neutral particle analyzer that views the heating beams are shown in figure 5; the signal is dominated by fast ions that charge exchange with injected neutrals in the core of the plasma. A high energy tail above the injection energy is evident for both 90 keV injection (figure 5(*a*)) and for 65 keV injection (figure 5(*b*)). Evidence of acceleration below the injection energy also appears in many of the spectra such as figure 5(*b*). Comparable fast-ion acceleration is observed for all five injection angles and energies. However, the energy increase for the later ($t = 0.3$ s) RF pulse is approximately 50% larger than that for the early pulse, even though the RF power is usually 0.5 MW greater for the early pulse. The analyzer is scanned between more parallel and more perpendicular angles shot-to-shot. The data from the pitch-angle scans

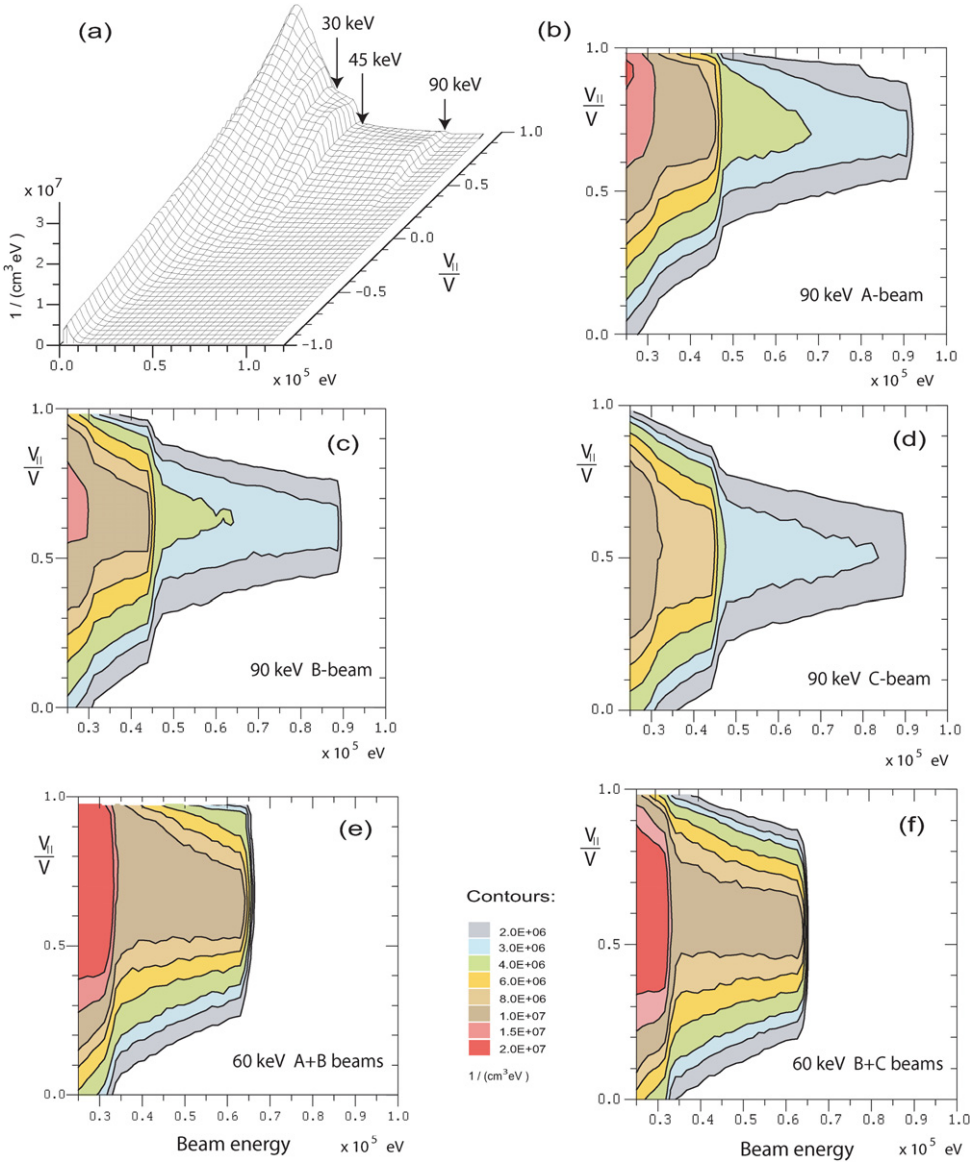

Figure 4. The volume-averaged fast-ion distribution function at 170 ms during injection of (*a*) (*b*) source A at 90 keV, (*c*) source B at 90 keV, (*d*) source C at 90 keV, (*e*) sources A and B at 65 keV, and (*f*) sources B and C at 65 keV. The distributions are calculated by the TRANSP Monte Carlo code [49] assuming neoclassical fast-ion behaviour.

(not shown) suggest the acceleration is strongest in the perpendicular direction, as expected for high-harmonic heating. The temporal evolution of the spectra indicate that the tail steadily grows during the 30 ms HHFW pulse. This is expected, since the HHFW acceleration competes with classical Coulomb collisions and the energy deceleration time for 90 keV fast ions under these conditions is ∼80 ms.

Neutron data confirm that fast ions are accelerated by the fast waves. The neutron rate increases rapidly during the HHFW pulse (figure 6). Some of the increase is due to changes in

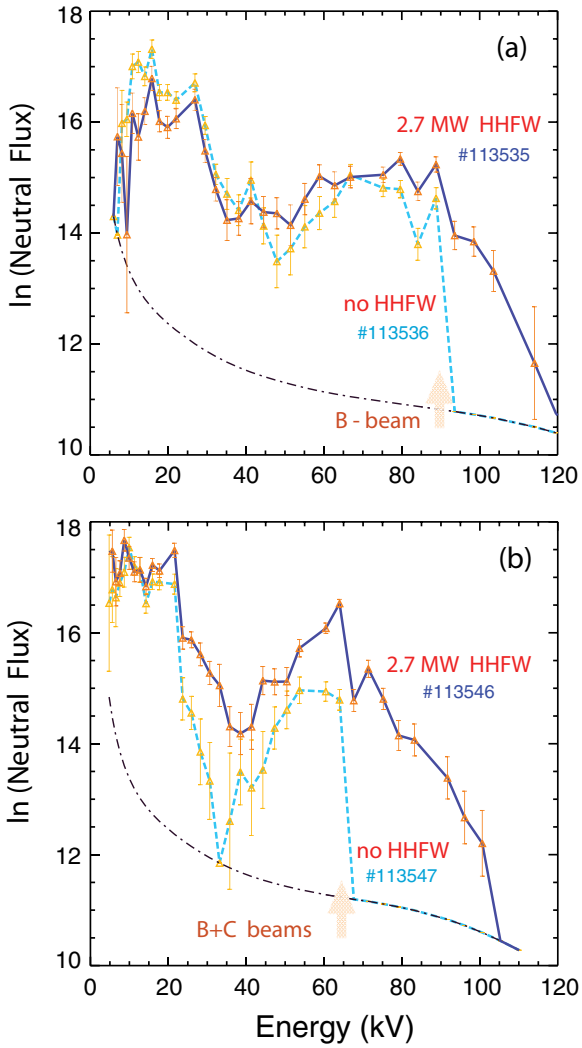

Figure 5. Neutral particle spectra measured by an E‖B analyzer [53] in nominally identical discharges with (——) and without (- - - -) HHFW heating. The spectra are measured at the end of the 30 ms duration HHFW pulse. (*a*) 90 keV injection by source B at 185 ms. Analyzer tangency radius of 70 cm. (*b*) 65 keV injection by sources B and C at 170 ms. Analyzer tangency radius of 50 cm. (The dash-dot line is the estimated noise floor for the measurement.)

Coulomb scattering but the increase is greater than classically expected (in the absence of wave heating). Since the neutron rate is dominated by beam–beam and beam–plasma reactions, this indicates that a significant fraction of high-energy fast ions are accelerated by the RF.

The observed perpendicular acceleration is expected theoretically. Because of the low magnetic field, the normalized gyroradius is large [$k_\perp \rho_f = O(10)$] and the cyclotron resonances are dense, so appreciable fast-ion absorption is expected throughout the plasma minor radius [51]. Figure 7 compares the fast-ion distribution function before RF to the distribution function after 30 ms of HHFW for one of the discharges with early RF heating. The distribution function is calculated from the Fokker–Planck equation by the CQL3D code [54].

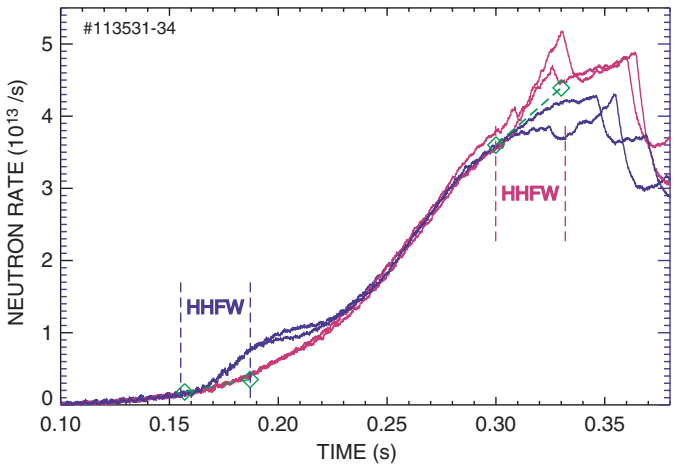

Figure 6. Neutron rate in four nominally identical discharges with a HHFW heating pulse either at 0.155–0.185 s or at 0.30–0.33 s. The increase in the neutron rate during the RF exceeds the expected classical increase associated with electron heating (dashed line between diamond symbols) because fast ions are accelerated by the waves. Source C is at 90 keV.

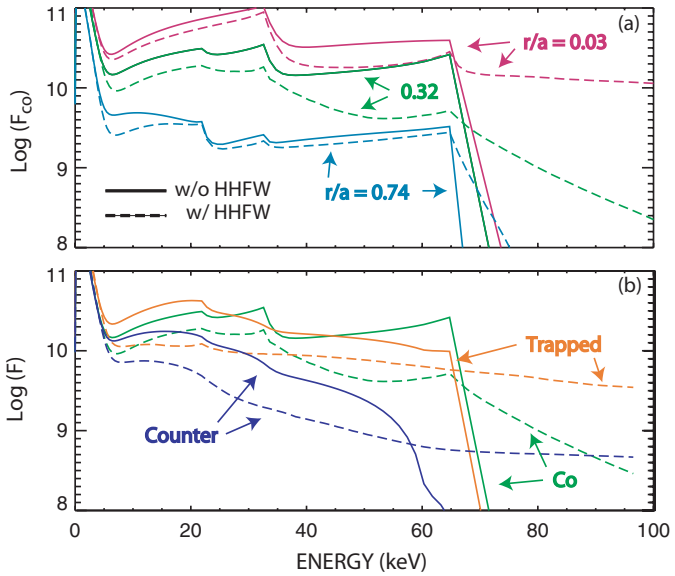

Figure 7. Energy distributions of fast ions before (solid) and after(dashed) a 30 ms HHFW heating pulse as calculated by the CQL3D [54] code for the discharge shown in figure 9 (#113546). (*a*) Distributions after averaging over pitch for co-circulating fast ions at three different values of normalized minor radius. (*b*) Distributions at $r/a = 0.32$ after averaging over pitch for the co-circulating, trapped and counter-circulating fast-ion populations.

In this calculation, the wave fields in the quasilinear RF operator Q are found using ray tracing (for the antenna parameters in [51]). The collision operator and beam source are computed from the measured plasma parameters and are assumed constant in the simulation. The simulated neutron rate increases a factor of ∼2.5 after 30 ms of HHFW, in fair agreement with the

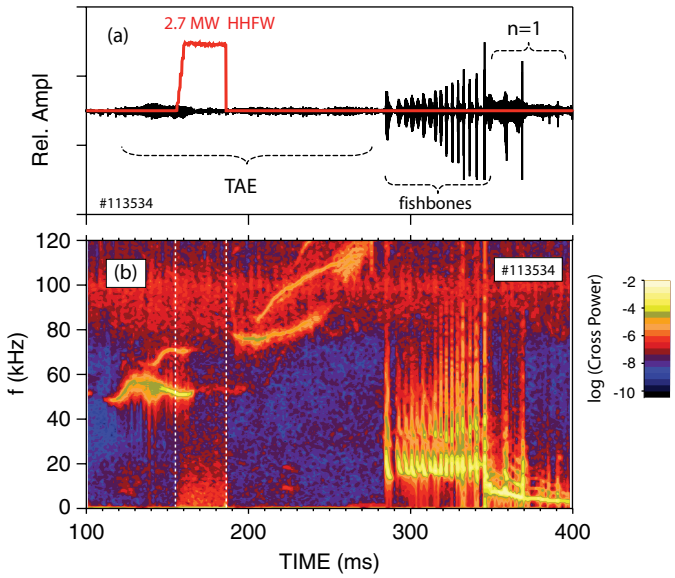

Figure 8. (*a*) Mirnov coil signal $\dot{B}$ that is mounted on the outer vacuum vessel wall and (*b*) its cross power with a probe that is displaced toroidally by 30°, plotted on a log base-10 scale. Modes in the TAE range of frequencies are excited early in the discharge and fishbones are excited later. In this discharge (and many others in the sequence), the confinement deteriorates when a fishbone triggers a large, low frequency $n = 1$ mode. The HHFW heating reduces the amplitude of the TAE activity in ∼10 ms in this particular example (shot #113534).

observed increase of ∼2.0. Examination of the simulated distribution function f reveals the following features.

- HHFW accelerates a substantial tail above the injection energy (figure 7), as measured experimentally (figure 5).
- As expected for a plasma with many resonant surfaces, acceleration occurs throughout the plasma. The tail is larger in the core than at the edge but appreciable tails occur at all radii. Figure 7 a shows spectra at three representative radii.
- Acceleration occurs for all pitch angles (not shown in figure 7, which shows pitch-angle averaged spectra for clarity).
- In the calculation, f decreases below the injection energy at all radii (figure 7). Evidently, the flux of fast ions to large energies depletes the phase-space density of lower energy ions. The measured neutral-particle spectra (figure 5) do not show this effect, however.
- As expected for perpendicular acceleration, the tail is largest for trapped particles (figure 7(*b*)). Depletion of the phase-space density below E_{inj} occurs for all classes of fast ions but is especially pronounced for passing particles that circulate in the direction of the plasma current (co-going ions).

3. Effect on instabilities

Several types of instabilities are readily apparent in the magnetics data (figure 8). Most of the discharges have steady-frequency modes in the 50–200 kHz range early in the discharge; we call these TAEs. Many of the discharges also have rapidly chirping instabilities in the same frequency band; this is the phenomenon dubbed Type II fishbones in [41]. Several examples

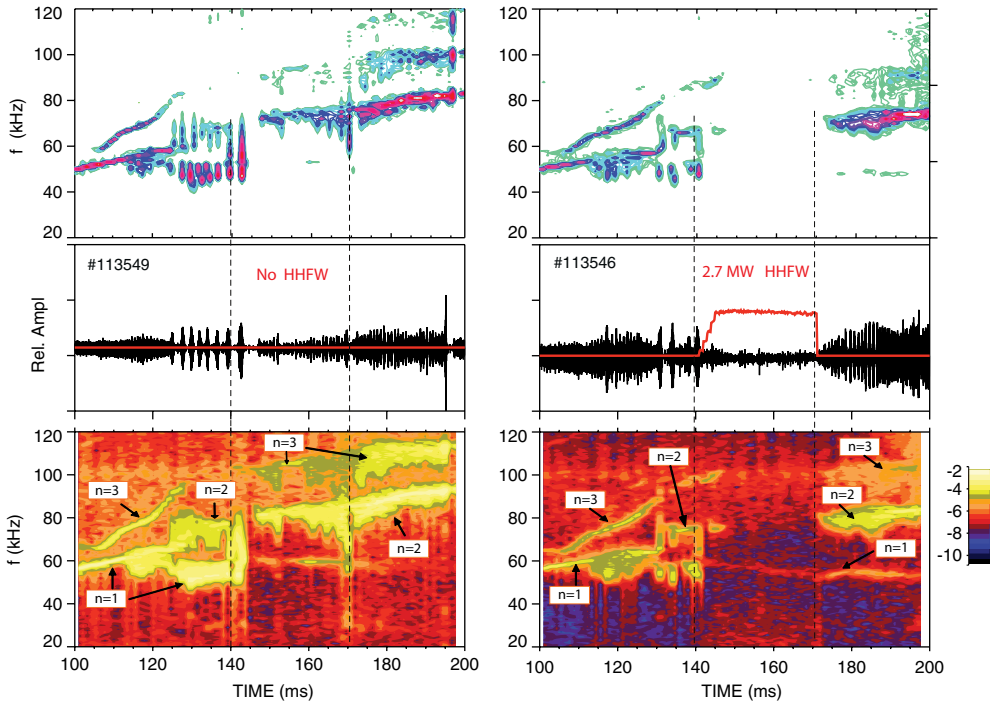

Figure 9. Comparison of the magnetics data in two nominally identical discharges with (right column) and without (left column) HHFW heating. The application of 2.7 MW of HHFW heating in the 140–170 ms time frame has a strong effect on the TAE activity. The suppression is evident in the amplitude spectrum of a single Mirnov signal (top row), the $\dot{B}$ signal itself (middle row), and the cross power spectrum, where several toroidal mode numbers n are indicated (bottom row). These two discharges were heated with 2 MW of 65 keV B and C beams.

appear in figure 9 between 130–140 ms. Later in the discharge (from 285–345 ms in figure 8), classic fishbones that whistle down in frequency from ∼25 to 10 kHz occur. In many of the discharges, a fishbone eventually triggers a low-frequency $n = 1$ instability. These low frequency modes gradually slow the plasma rotation and often cause a disruption; an example appears from 345–400 ms in figure 8. In addition, all the discharges exhibit CAE or GAE activity in the 0.6–1.4 MHz frequency range (not shown in figure 8).

3.1. TAE-band instabilities

The early MHD activity depends on the neutral beam injection parameters. When source A is injected at 90 keV, a strong burst cycle of repetitive Type II fishbones develops around 150 ms (figure 10). Although chirping modes in this frequency band are sometimes observed with the other four beam combinations (as in figure 9 at 135 ms), strong repetitive chirping is only observed with the most tangential source at full energy (source A at 90 keV). For the other beam parameters, steady-frequency modes predominate.

Figure 11 shows the spatial structure of the Alfvén continuum early in the discharge when the steady-frequency TAEs appear. As expected for an elongated, high-beta spherical tokamak, the gaps in the continuum are quite large throughout most of the plasma. Globally extended modes with minimal continuum damping are theoretically possible for most frequencies. The modes with steady frequencies of 50–200 kHz lie in the TAE gap throughout the

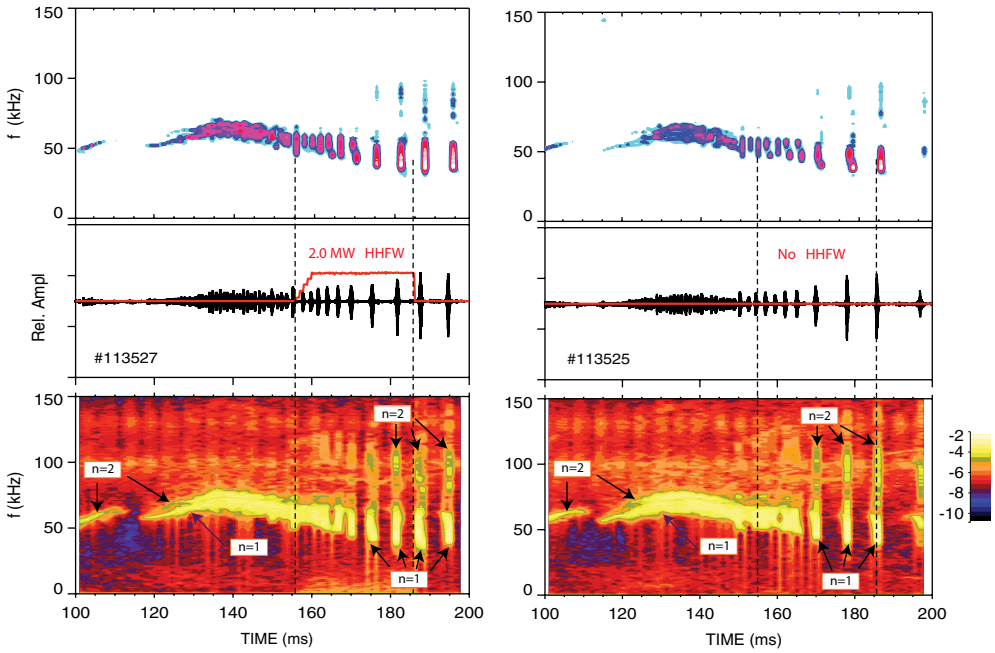

Figure 10. Comparison of the magnetics data in two nominally identical discharges with (left column) and without (right column) HHFW heating during repetitive chirping activity in the TAE frequency band. The application of 2.0 MW of HHFW heating has no detectable effect on the chirping modes. The amplitude spectrum of a single Mirnov signal (top row), $\dot{B}$ signal (middle row), and cross power spectrum are shown. The dominant ∼50 kHz modes are $n = 1$. These two shots were heated with 2 MW of 90 keV A beams.

outer half of the plasma. (The toroidal rotation frequency in the outer half of the plasma is only a few kHz early in the discharge, so the Doppler shift correction is small there.) Unfortunately, internal measurements of the instability eigenfunctions are unavailable early in the discharge. Reflectometer measurements at intermediate times (269 ms) [55] are consistent with identification of the steady modes as TAEs.

Application of HHFW early in the discharge often alters the steady TAE activity. One of the clearest examples of this is shown in figure 9. When the HHFW power is applied, the TAE and weakly-chirping modes (frequency sweeps $\Delta f/f \lesssim 10\%$) drop in amplitude by at least two orders of magnitude. The amplitude decays with a few millisecond delay at the beginning of the HHFW pulse and recovers a few milliseconds after the heating terminates.

In contrast, the application of HHFW has no discernible effect on strongly-chirping instabilities ($\Delta f/f > 20\%$) in the TAE band. Figure 12 details the activity when the HHFW turns off. The frequency of the $n = 1$ modes chirps downwards linearly in time from ∼57 to ∼32 kHz in 0.3 ms irrespective of the RF heating.

3.2. Fishbone instabilities

The chirping modes that occur late in the discharge have the features of classic fishbones (figure 13). Like the fishbones that were driven by trapped fast ions in the poloidal divertor experiment (PDX), there is a regular cycle of instability bursts and drops in the neutron rate [5]. The mode is $n = 1$. In the absence of internal magnetic field measurements, the equilibrium

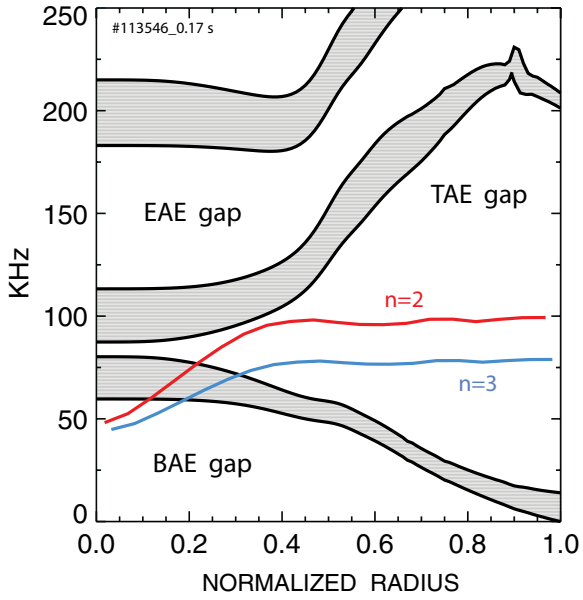

Figure 11. Alfvén gap structure for shot #113546 at $t = 169$ ms as calculated by the CONT code in the 'slow-sound' approximation [60]. The dark bands represent the continuum. The elongation-induced (EAE), toroidicity-induced (TAE), and beta-induced (BAE) gaps are indicated. The Doppler-corrected frequency of two observed instabilities, $f_{\rm plasma} = f_{\rm lab} - nf_{\rm rot}$, is also shown. ($f_{\rm rot}$ is the rotation frequency of carbon as measured in a similar discharge.)

reconstructions have substantial uncertainty but it is plausible that q_0 drops below unity; the activity begins just as $q_0 \to 1$. The signals from central soft x-ray chords closely resemble the evolution in classic fishbones. The frequency chirp also closely resembles the behaviour in classic PDX fishbones.

Application of HHFW late in the discharge has no discernible effect on the fishbone activity (figure 14). Any changes associated with the radio frequency waves are smaller than the shot-to-shot variability in MHD activity. Figure 15 details the activity when the HHFW turns off. The frequency of the $n = 1$ modes chirps downwards linearly in time from ∼28 to ∼15 kHz in 0.4 ms irrespective of the RF heating.

3.3. MHz-band instabilities

Rich spectra in the MHz-frequency band occur in all of the discharges. Usually some of the modes have steady frequencies, while others exhibit frequency chirping. In figure 16, the ∼1.1 MHz mode at 160 ms illustrates a steady-frequency mode, while the vertically elongated band of ∼0.85 MHz modes at 140 ms illustrates typical chirping behaviour. The spectra probably contain an admixture of CAEs and GAEs. As usual in NSTX, the mode frequencies are ∼0.2 MHz higher for source C than for source A, as expected for the Doppler-shifted cyclotron resonance that drives the instabilities [44]. In this frequency band, frequency chirping occurs in several discharges for a number of different injection angles and energies. An example from a discharge with 90 keV beam injection by source A is shown in figure 17. In contrast to the lower-frequency modes (figures 12 and 15), many of the MHz-frequency bursts exhibit the $\sqrt{\delta t}$ frequency sweep predicted by perturbative BB theory (equation (1)). In this example, HHFW heating has no effect on the evolution of the chirping instabilities. In other

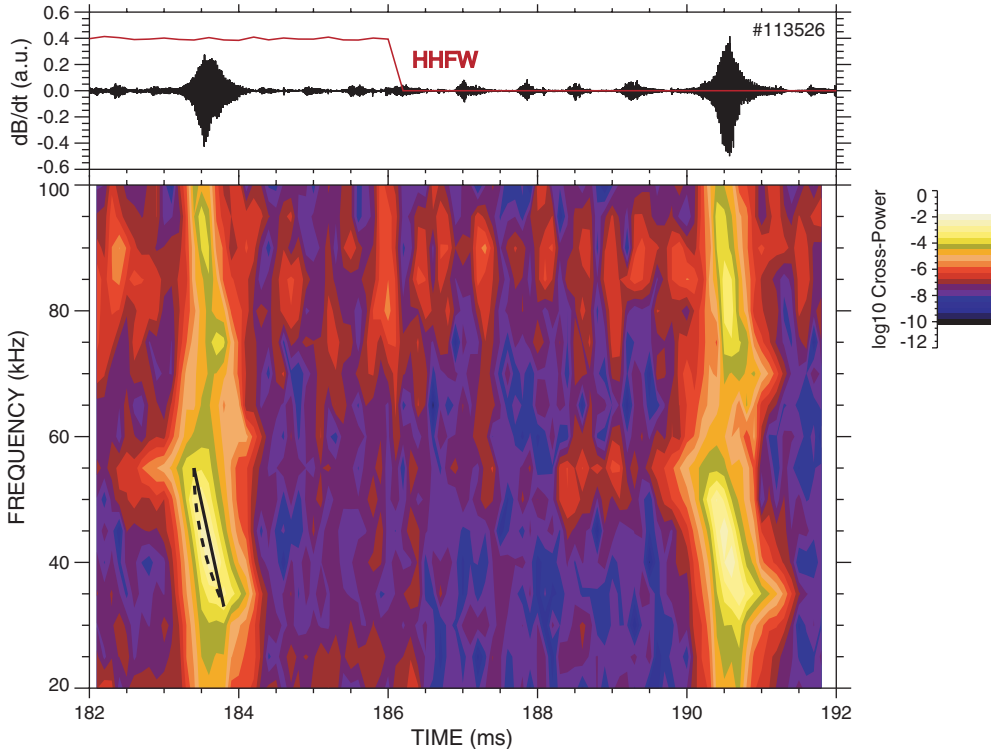

Figure 12. Magnetics signal and spectra at the end of the RF pulse for a discharge with repetitive chirping activity in the TAE frequency band. The solid and dashed lines that are superimposed on the frequency chirp near 184 ms represent a linear (equation (2)) or $\sqrt{\delta t}$ (equation (1)) dependence of the frequency on time, respectively. HHFW power of 1.3 MW; 2 MW of 90 keV A beams.

cases (figure 18), the frequency sweep Δf of most bursts is shorter during the HHFW pulse. Changes such as the one shown in figure 18 occur in several discharges but the changes do not occur reproducibly for a given condition. More data are needed to determine unambiguously if HHFW heating alters the frequency chirping in the MHz frequency band.

3.4. Summary

Here is a summary of the experimental observations.

- Classic fishbones occur in all discharges with all beam combinations; these modes are unaffected by HHFW heating.
- Strong 'Type II' chirping modes occur most often with high energy, tangential (90 keV source A) injection. These are unaffected by HHFW heating.
- CAE and/or GAE modes occur with all beam combinations. When repetitive chirping occurs, HHFW heating may have an effect but the evidence is ambiguous.
- Steady frequency modes in the TAE band are partially stabilized by HHFW heating. The effect develops on a 1–10 ms timescale.

A compilation of the effect of HHFW heating in all of the discharges appears in figures 19 and 20. In these figures, a discharge like figure 9 is categorized as a 'Strong' effect, while the effect for a case like figure 14 is called 'None.' The effect is categorized as 'Weak' if a change

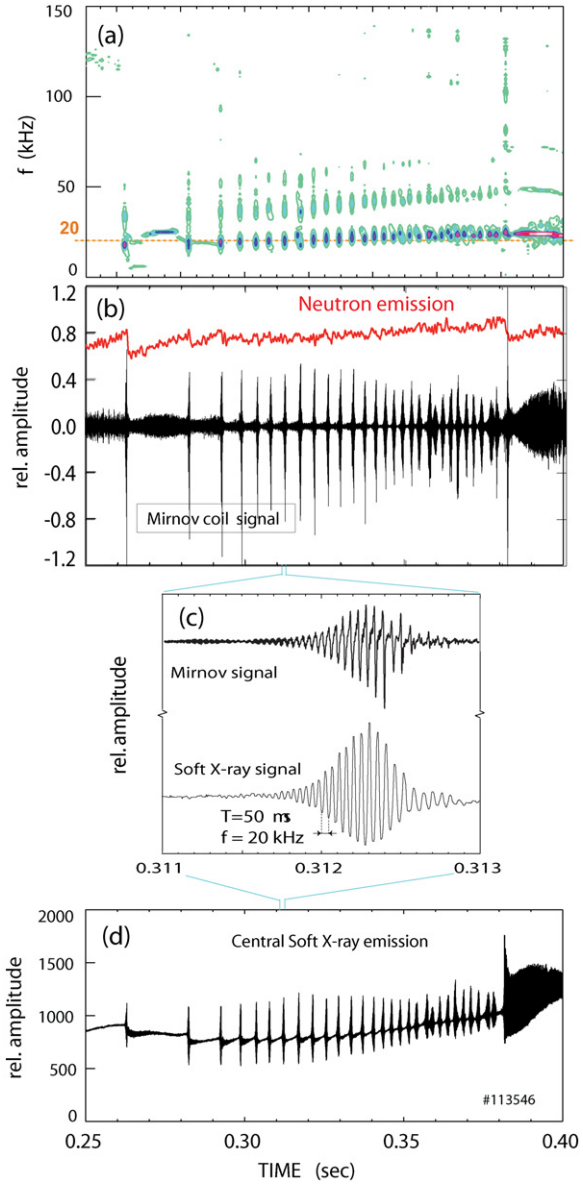

Figure 13. Data during the fishbone activity late in discharge #113546 as q_0 approaches unity. (*a*) Mirnov signal amplitude spectrum, (*b*) $\dot{B}$ Mirnov signal together with the neutron rate, showing substantial neutron drops early in the fishbone cycle, (*c*) details of Mirnov and soft x-ray signal, and (*d*) central soft x-ray emission with its characteristic fish skeleton shape.

is discernible but the change is comparable to the intrinsic shot-to-shot variability. Irrespective of beam-injection angle or energy, the HHFW pulse has no effect on classic fishbones or strong early chirping modes (figure 19). In contrast, steady-frequency modes in the TAE band are nearly always diminished by the HHFW pulse. This is true for both cases with 65 keV injection and for injection with source C at 90 keV. The most ambiguous case is source B at 90 keV: sometimes HHFW has a clear effect and sometimes it does not. It is not surprising

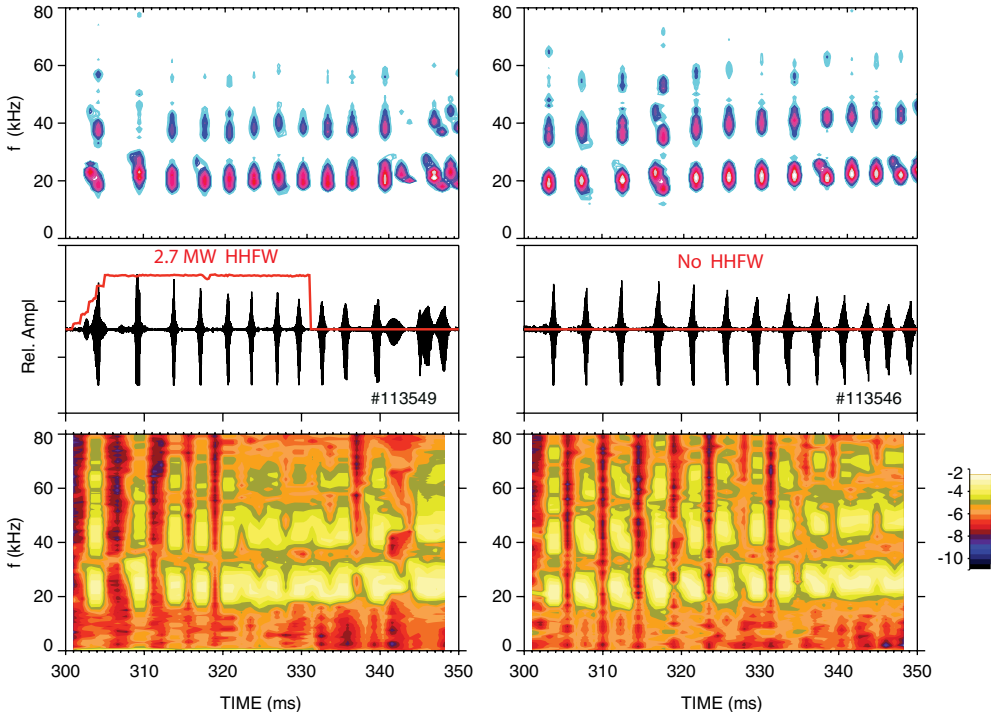

Figure 14. Comparison of the magnetics data in two nominally identical discharges with (right column) and without (left column) HHFW heating during strong fishbone activity. The application of 2.7 MW of HHFW heating has no detectable effect on the fishbones. The amplitude spectrum of a single Mirnov signal (top row), $\dot{B}$ signal (middle row), and cross power spectrum are shown. The ∼22 kHz mode is $n = 1$ and the ∼42 kHz peak is a $n = 2$ harmonic. These two shots were heated with 2 MW of 65 keV B and C beams.

that the behaviour for source B is intermediate between source C where the effect is strong and source A where there is no effect.

The effect of the HHFW does not correlate with the toroidal mode number and frequency of the instability (figure 20). Steady modes of all toroidal mode numbers and frequencies are affected by the HHFW, while no low-frequency chirping mode of any type is altered by the HHFW pulse.

4. Discussion

Prior to the experiment, we expected HHFW acceleration to modify the chirping behaviour but have little effect on steady-frequency modes. The objective of this section is to explain why the observations contradict our initial hypothesis.

4.1. Nature of the instabilities

A difficulty in the interpretation of the effect of the HHFW on the evolution of the instabilities is that the linear stability of the various instabilities is imperfectly understood. Because the 50–100 kHz modes are in the TAE frequency band, resemble TAEs in other devices [42], and there is a strong correlation between mode activity and beam-injection parameters, the

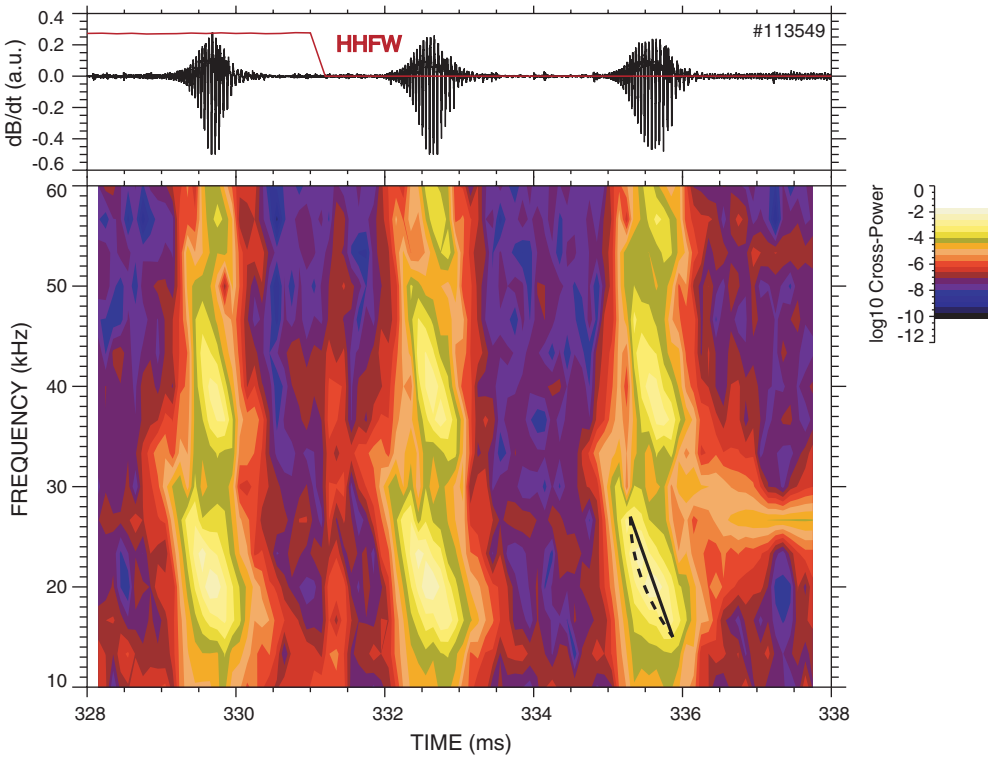

Figure 15. Magnetics signal and spectra at the end of the RF pulse for the discharge shown in figure 14. The solid and dashed lines that are superimposed on the frequency chirp near 336 ms represent a linear (equation (2)) or $\sqrt{\delta t}$ (equation (1)) dependence of the frequency on time, respectively.

modes are thought to be driven by fast ions but it is not known which portion of the fast-ion distribution function resonates with the instability. (More detailed measurements of the fast-ion distribution function are needed to determine this.) Previous calculations suggest that these modes resonate with the bounce motion of trapped ions [56]. However, in this experiment, the modes are driven most strongly by the most tangential source, suggesting that a resonance with passing ions is important. Measurements of the spatial structure are limited but suggest that the eigenfunction extends over much of the plasma [55].

For the classic fishbones, measurements of the spatial structure by soft x-ray and reflectometer diagnostics [55] indicate that the mode amplitude is large in the plasma core. No phase inversion is observed in the soft x-ray data, which is consistent with identification of the mode as an ideal kink. Theoretically, it appears likely that trapped fast ions drive the instability [56]. The fact that the neutron rate drops rapidly at the fishbone bursts implies that high-energy ions are expelled or redistributed by the waves [57]. In addition to the free energy derived from fast ions, it is likely that the ideal MHD drive associated with q_0 dropping below unity plays an important role in the burst dynamics.

The identification of the chirping MHz modes is uncertain in this experiment. Subsequent polarization measurements with an improved set of magnetic diagnostics show conclusively that both GAEs and CAEs can chirp in NSTX. If the chirping modes in this experiment are CAEs, then their radial eigenfunction is probably radially and poloidally localized near

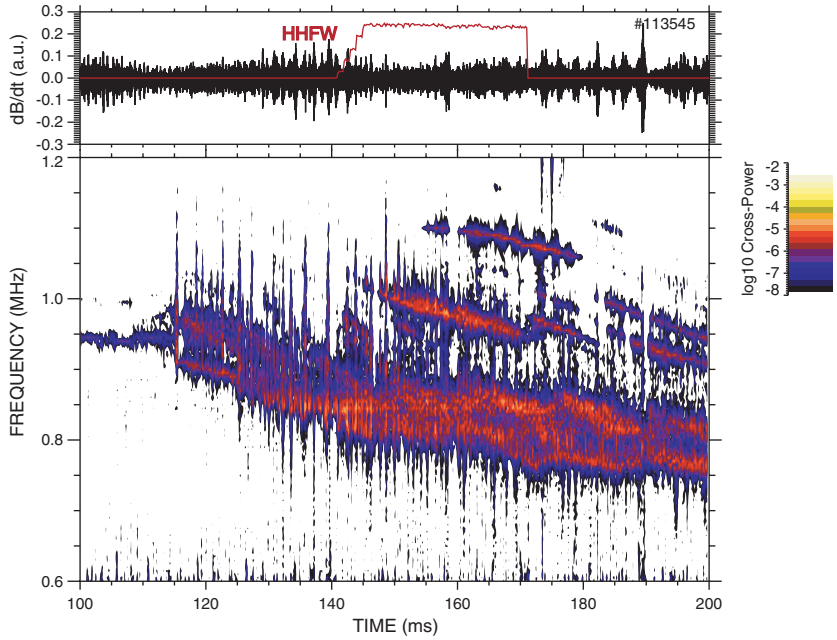

Figure 16. Representative magnetics signal and spectra in the MHz-frequency band. HHFW power of 2.7 MW; sources A and B at 65 keV.

the midplane at a normalized minor radius of ∼0.8 and the fast ions that drive the modes are probably large banana-width, trapped ions that experience a Doppler-shifted cyclotron resonance with the wave [44].

4.2. Empirical interpretation in terms of trapped/passing populations

Our empirical interpretation begins with the assumption that repetitive chirping occurs when a mode is driven strongly by the fast-ion population. For a weak drive that barely exceeds the damping, a steady frequency with only slight amplitude variation is possible but, as the drive grows, a burst cycle develops. This behaviour is often observed experimentally [1] and is consistent with both the semi-empirical predator–prey model [25] and the BB model. If this assumption is correct, the early TAE-band instabilities are driven most strongly by source A at full energy (strong Type II fishbones), followed by source B at full energy (occasional chirping), followed by the other beam conditions (steady modes with occasional small frequency chirps of $\Delta f/f \lesssim 20\%$). Notice that we are implicitly assuming that the steady-frequency TAEs and the Type II fishbones are essentially the same *linear* instability but have different nonlinear dynamics. The fact that source A (the most tangential source) provides the strongest drive suggests that these modes are driven by fast ions with large parallel velocity. The addition of HHFW heating adds perpendicular energy to the fast ions and shifts their pitch angles to lower values, converting some passing particles to trapped particles; it also accelerates fast ions to speeds well above the Alfvén speed. In the case of the steady-frequency, weakly driven modes, this reduction in passing particles has a strong effect on the linear drive γ_L and the mode is nearly stabilized. The stabilization occurs gradually, however, because it takes several milliseconds to alter the distribution function significantly. In contrast, for the chirping modes that are driven by a robust passing population, perpendicular heating of the fast ions has no discernible effect on the mode evolution.

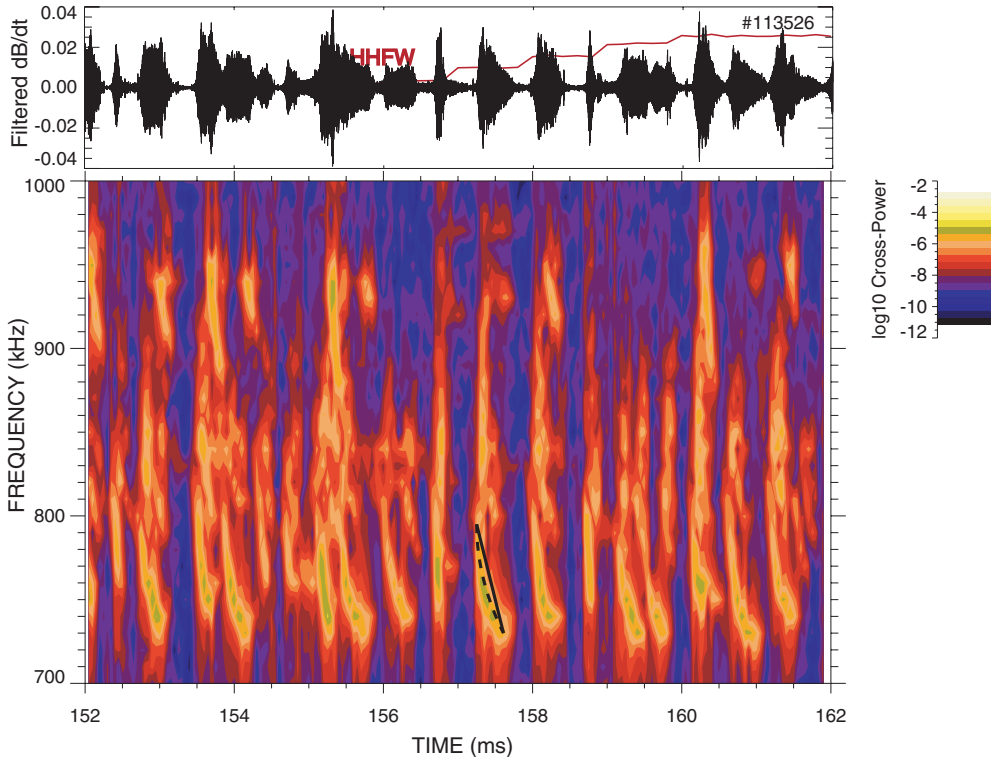

Figure 17. Magnetics signal and spectra at the beginning of the RF pulse for a discharge with repetitive chirping activity near 1 MHz. The signal is digitally high-pass filtered at a cutoff frequency of 0.68 MHz. The solid and dashed lines that are superimposed on the frequency chirp near 158 ms represent a linear (equation (2)) or a $\sqrt{\delta t}$ (equation (1)) dependence of the frequency on time, respectively. HHFW power of 1.3 MW; 2 MW of 90 keV A beams.

The classic fishbones are probably driven by MHD and by the trapped particle population. HHFW heating has no effect in this case because the modes are very strongly driven and because the heating acts to *increase* γ_L by increasing the trapped particle population.

HHFW heating may have affected the chirping of the MHz instabilities. Of the chirping instabilities in this experiment, the MHz modes may have been the most weakly driven. These modes were the only ones to follow the perturbative frequency scaling during a burst (equation (1)), $\delta\omega \propto \sqrt{t}$. Also, even for nominally identical discharges, the chirping behaviour did not occur on every shot, suggesting the modes were close to a threshold. These modes are thought to be produced by trapped fast ions with orbits that span from the plasma centre to the outer portion of the plasma [44], so HHFW acceleration should alter the effective collisionality of the fast ions that resonate with the mode.

Quantitative estimates of these effects can be obtained from the distribution functions calculated by the CQL3D code (figure 7). Consider first the TAE. The fundamental resonance with passing particles occurs when $v_\parallel = v_A$. Integration of the distribution function over the particles that satisfy the resonance condition shows that the number of resonant particles decreases by a factor of two throughout most of the plasma by the end of a 30 ms HHFW heating pulse. In a conventional high-field tokamak, RF heating generally *increases* the instability drive by increasing the number of high-energy trapped ions that resonate with the

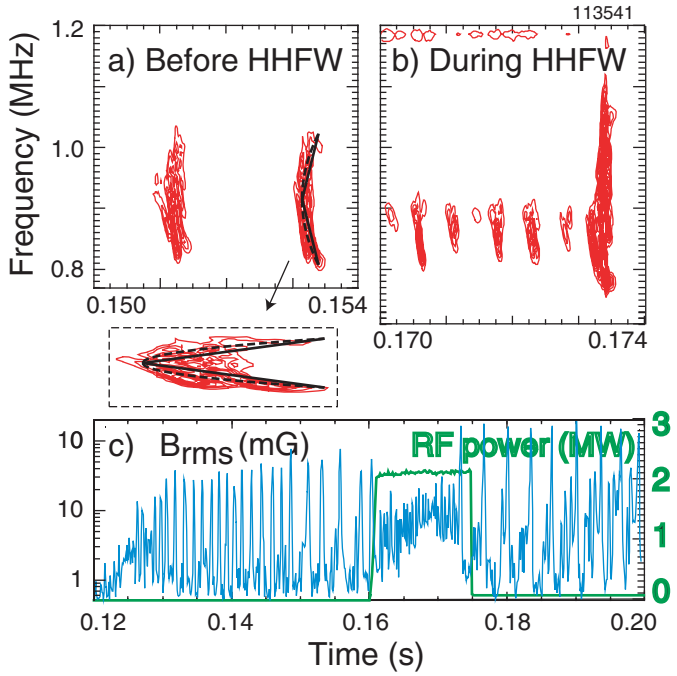

Figure 18. Magnetics spectrogram (*a*) before and (*b*) during HHFW heating and (*c*) rms magnetic fluctuation level in the high-frequency band and HHFW power in a discharge with 2 MW of 90 keV B beams. The dashed box compares the evolution of the frequency chirp at 153 ms with a linear or a $\sqrt{\delta t}$ dependence of the frequency on time.

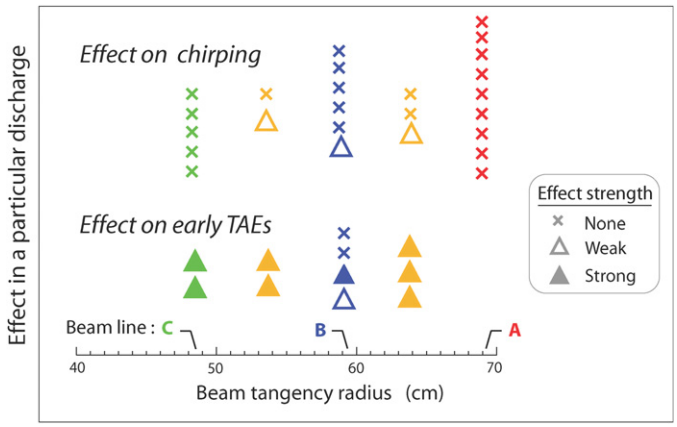

Figure 19. The effect of the beam tangency radius on early TAE modes and late fishbones for all of the discharges in the experiment. Each symbol represents a discharge. When two beam lines are used, the median value of their tangency radius is shown. Early TAEs are not observed with source A at 90 keV.

mode. The situation is different in NSTX. Because of the low field, the fundamental resonance corresponds to a relatively low parallel energy of only $\frac{1}{2}mv_{\parallel}^2 \simeq 22\,\mathrm{keV}$. The high-harmonic heating causes diffusion in energy that reduces the number of intermediate-energy passing ions, thereby weakening the instability drive. A similar calculation for the Doppler-shifted

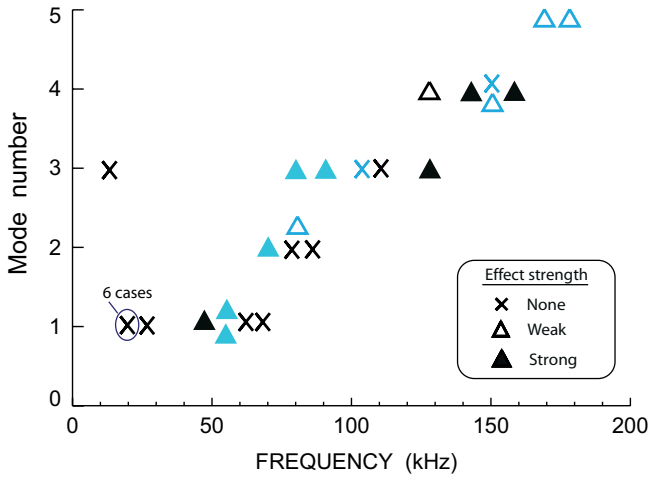

Figure 20. The effect of HHFW heating on early TAEs as a function of toroidal mode number n and frequency for all of the discharges in the experiment. Black (blue) symbols represent injection at 90 (65) keV.

cyclotron resonance ($\omega = \omega_{ci} - k_{\|} v_{\|}$) shows that the number of trapped resonant ions at $r/a \simeq 0.8$ increases slightly, so HHFW heating should have little effect on the linear stability of the CAE. For the fishbone instability, trapped particles inside the $q = 1$ surface are the dominant drive. In this case, the calculated number of trapped ions in the inner third of the plasma increases slightly with HHFW heating, so the RF should be weakly destabilizing.

4.3. Interpretation in terms of the BB model

HHFW heating does not suppress the frequency chirping of the low frequency instabilities. Within the framework of the BB model, there are three likely explanations.

- The ions that resonate with the instabilities are in a different part of phase-space than the ions that interact with the HHFW.
- The increase in the effective collision frequency ν_{eff} was too small to alter the nonlinear dynamics.
- The frequency chirp arises from nonperturbative energetic particle effects unrelated to the formation of phase-space structures.

The resonant ions that drive the instabilities occupy a particular volume in phase-space, i.e. they have a certain energy, pitch angle, and spatial location. Theoretically, HHFW absorption in NSTX occurs broadly in both velocity space and configuration space [51] (figure 7). For the classic fishbones it is virtually certain that the instability and the RF interact in the same portion of phase-space. Both the instability and the RF cause changes in neutron rate, demonstrating overlap with the high-energy population. The NPA measurements indicate acceleration near the plasma centre, in the same region where the soft x-ray diagnostic measures strong fluctuations. The situation is less certain for the chirping TAE instabilities but, given the broad nature of the HHFW heating, some interaction with the resonant ions seems likely.

A second possible explanation is that the stochastic heating of the resonant ions by the RF is too small. At first glance, this explanation seems unlikely. In the dipole experiment [17] that motivated our experiment, only 40 W of cyclotron heating was required to suppress frequency chirping. ($\sim$1 kW of power formed the fast-electron population.) The HHFW power is much

larger ($\gtrsim$2 MW) in our experiment and is comparable to the heating power. However, an important difference is that electron cyclotron heating is more localized spatially than HHFW heating. Nevertheless, even taking into account the differing volumes and densities of the two experiments, the power density per energetic particle is at least an order of magnitude larger in our NSTX experiment. Empirically, it is surprising that frequency chirping is not suppressed.

Quantitative estimates suggest that the stochastic diffusion of the ions that resonate with the instabilities was marginal. To suppress chirping, the stochastic heating must 'kick' the resonant ions out of the potential well formed by the instability. In other words, the RF must change the particle orbit sufficiently that it is no longer trapped by the mode. Thus, to affect the viability of the hole structure during the chirp, we need

$$(\delta E/E_{\mathrm{r}})^2 \gtrsim (\omega_{\mathrm{b}}/\omega)^2, \tag{3}$$

where δE is the energy spread associated with stochastic diffusion, E_{r} is the energy of fast ions that resonate with the instability, ω_{b} is their trapping frequency in the finite amplitude instability, and ω is the mode frequency. Let us estimate each of these quantities for the fishbone instability. Cyclotron heating imparts perpendicular energy to the ions. The energy spread δE induced by the RF in a time t is

$$(\delta E)^2 \sim D_E t, \tag{4}$$

where D_E is the energy diffusion coefficient. The magnitude of D_E is readily estimated from the neutral particle data which show that an energy spread of about 40 keV occurs in 30 ms, so $D_E \sim 5 \times 10^4\,(\mathrm{keV})^2\,\mathrm{s}^{-1}$. The frequency chirp lasts about 0.3 ms, so $(\delta E/E_{\mathrm{r}})^2 \simeq 0.01$. To estimate ω_{b}, we use the measured mode amplitude in a NOVA-K simulation that computes the average trapping frequency of the fast ions [58]. For the fishbone, the measured amplitude [45] is $\tilde{n}_e/n_e \sim 0.01$, both trapped and passing fast ions contribute to the resonance, and the computed trapping frequency in the $n = 1$ mode is $\omega_{\mathrm{b}} = 1.2 \times 10^4\,\mathrm{rad\,s}^{-1}$. Accordingly, the right-hand side of equation (3) is $O(0.01)$, so the RF-induced stochasticity is of the correct order of magnitude to have an effect but may have been inadequate.

For the TAE, a NOVA-K calculation of a $n = 4$ mode with measured amplitude [45] of $\tilde{n}_e/n_e \sim 10^{-3}$ gives a trapping frequency of $3.5 \times 10^4\,\mathrm{rad\,s}^{-1}$. In this case, the primary resonance is between passing particles and the mode, so it is the canonical toroidal angular momentum P_ϕ that determines the resonance condition. For cyclotron absorption, the relationship between a change in perpendicular energy and the change in P_ϕ is [59]

$$\delta P_\phi = \frac{n_{\mathrm{RF}}}{\omega_{\mathrm{RF}}}\delta E, \tag{5}$$

where n_{RF} and ω_{RF} are the toroidal mode number and frequency of the HHFW. The canonical toroidal angular momentum is $P_\phi = Rmv_\phi + eRA_\phi$. Substituting typical values of magnetic vector potential of $0.06\,\mathrm{T\,m}^{-1}$, $R \simeq 1\,\mathrm{m}$, and $Rmv_\phi \simeq R_{\tan}\sqrt{2mE} \simeq 0.03\,\mathrm{eV\,s}^{-1}$, $n_{\mathrm{RF}} \simeq k_\parallel R \simeq 14$, and $\omega_{\mathrm{RF}}/(2\pi) = 30\,\mathrm{MHz}$, we find that $(\delta P_\phi/P_\phi)^2 \simeq 0.01$. This is to be compared with $(\omega_{\mathrm{b}}/\omega)^2 \simeq 0.01$. As for the fishbone instability, this implies that the HHFW heating is of the right order of magnitude to alter the phase-space structure but may have been insufficient. For both the fishbone and the TAE, these estimates have large uncertainties associated with uncertainty in the mode amplitude and structure, the proper choice of resonant ions for the trapping calculation within NOVA-K, and the relationship between the empirical estimate of D_E and the acceleration of the fast ions that actually drive the instabilities.

In the dipole experiment, chirping suppression was only observed when the cyclotron heating was resonant at major radii outside of the hot electron ring [18]. It was also found that the extent of the frequency chirp Δf depended on the location of the cyclotron resonance layer. The proposed interpretation of these results is that, since the interchange instability drives

resonant electrons outward, the ECR only affects chirping if the phase-space hole propagates through the cyclotron resonance layer. This suggests a possible explanation for the failure of the HHFW to suppress chirping in our experiment. Although our zero-dimensional estimates indicate that the RF power was in the range to have an effect, perhaps the fast waves failed to suppress chirping because the resonant structures in phase-space did not traverse portions of phase-space with sufficiently strong fast-ion absorption.

5. Conclusion

In contrast to initial expectations, high-power cyclotron heating has no effect on the nonlinear dynamics of two fast-ion driven instabilities and only a weak effect (if any) on a third. The RF waves do accelerate fast ions, however. The RF also improves the stability of TAEs, probably by reducing the phase-space density of the intermediate-energy fast ions that drive the instability.

We had attributed the frequency chirps to the formation of phase-space structures. Sufficiently strong particle orbit stochasticity induced by RF would destroy these structures during the time interval of a chirp. As such a change was not observed, one can question whether there was enough RF power to produce the needed stochasticity or whether the interpretation that the chirping is due to the formation of phase-space structures, in the form of holes and clumps, is correct.

With regard to whether there is enough RF power, a rough estimate of the characteristic lifetime of a chirping phase-space structure shows that the lifetime is comparable to the time of the observed chirps (section 4.3). This result indicates that the experimental power is close to what is needed to see an effect, but as the estimate is rough, it could well be that there was not quite enough RF power to produce an effect.

A possibility remains that the observed chirping is not due to the formation of phase-space structures. For example, it is possible that chirping of one or more of these instabilities is caused by avalanche phenomena of non-perturbative waves. In such a case the waves have linear frequencies that are sensitive to the hot particle distribution function rather than to the formation of holes and clumps. In this case a redistribution of the hot particles due to the finite amplitude of the wave can conceivably cause the large frequency shifts being observed. If this were the case, the observed chirping would not be sensitive to particle stochasticity induced by the RF.

In future experiments, two improvements are needed to distinguish between these possibilities. First, detailed measurements of the fast-ion distribution function should ascertain which fast ions interact with the instabilities and the stochastic acceleration of those particular fast ions by the RF. Second, a more focused heating technique should create more stochastic diffusion with less perturbation of the background plasma. In our initial conception of this study, HHFW was considered an attractive heating technique because it interacts with a large portion of the fast-ion phase-space, virtually guaranteeing acceleration of the relevant fast ions. In hindsight, rather than the 'blunderbuss' of HHFW, the 'scalpel' of a heating technique that focuses its power in a narrow portion of phase-space is better suited to a definitive test of the applicability of the BB model to these chirping instabilities.

Acknowledgments

The assistance of R Bell, N Crocker, D Darrow, S Kaye, K Tritz, R Wilson and the entire NSTX team is gratefully acknowledged. This work was supported by United States Department of Energy Grant DE-FG02-05ER54681.

References

[1] Heidbrink W W and Sadler G J 1994 *Nucl. Fusion* **34** 535
[2] Wong K L *et al* 1991 *Phys. Rev. Lett.* **66** 1874
[3] Heidbrink W W, Strait E J, Doyle E, Sager G and Snider R T 1991 *Nucl. Fusion* **31** 1635
[4] Chen L 1994 *Phys. Plasmas* **1** 1519
[5] Mcguire K *et al* 1983 *Phys. Rev. Lett.* **50** 891
[6] Heidbrink W W 1995 *Plasma Phys. Control. Fusion* **37** 937
[7] Gryaznevich M P and Sharapov S E 2000 *Nucl. Fusion* **40** 907
[8] Kusama Y *et al* 1999 *Nucl. Fusion* **39** 1837
[9] Shinohara K *et al* 2001 *Nucl. Fusion* **41** 603
[10] Toi K *et al* 2000 *Nucl. Fusion* **40** 1349
[11] Kolesnichenko Y I *et al* 2005 *Phys. Rev. Lett.* **94** 165004
[12] Sharapov S E *et al* 1999 *Nucl. Fusion* **39** 373
[13] Snipes J A *et al* 2000 *Plasma Phys. Control. Fusion* **42** 381
[14] Wong K L *et al* 2000 *Phys. Rev. Lett.* **85** 996
[15] Valovic M *et al* 2000 *Nucl. Fusion* **40** 1569
[16] Liu Y *et al* 2004 *Nucl. Fusion* **44** 372
[17] Maslovsky D, Levitt B and Mauel M E 2003 *Phys. Rev. Lett.* **90** 185001
[18] Maslovsky D, Levitt B and Mauel M E 2003 *Phys. Plasmas* **10** 1549
[19] Bernstein I B, Greene J M and Kruskal M D 1957 *Phys. Rev.* **108** 546
[20] Berk H L, Breizman B N and Ye H 1992 *Phys. Rev. Lett.* **68** 3563
[21] Berk H L, Breizman B N and Pekker M 1996 *Phys. Rev. Lett.* **76** 1256
[22] Berk H L, Breizman B N, Candy J, Pekker M and Petviashvili N V 1999 *Phys. Plasmas* **6** 3102
[23] Vann R G L, Dendy R O, Rowlands G, Arber T D and D'Ambrumenil N 2003 *Phys. Plasmas* **10** 623
[24] Berk H L, Breizman B N and Petviashvili N V 1997 *Phys. Lett.* A **234** 213
Berk H L, Breizman B N and Petviashvili N V 1998 *Phys. Lett.* A **238** 408 (erratum)
[25] Heidbrink W W *et al* 1993 *Phys. Fluids* B **5** 2176
[26] Berk H L, Breizman B N and Pekker M 1995 *Phys. Plasmas* **3** 1826
[27] Wong K L *et al* 1997 *Phys. Plasmas* **4** 393
[28] Wong K-L 1999 *Plasma Phys. Control. Fusion* **41** R1
[29] Fasoli A *et al* 1998 *Phys. Rev. Lett.* **81** 5564
[30] Heeter R F, Fasoli A F and Sharapov S E 2000 *Phys. Rev. Lett.* **85** 3177
[31] Pinches S D *et al* 2004 *Plasma Phys. Control. Fusion* **46** S47
[32] Vann R G L, Dendy R O and Gryaznevich M P 2005 *Phys. Plasmas* **12** 032501
[33] Gryaznevich M P *et al* 2006 *Nucl. Fusion* **46** at press
[34] Boswell C J *et al* 2006 *Phys. Rev. Lett.* **96** submitted
[35] Vann R G L, Dendy R O, Gryaznevich M and Sharapov S E 2006 Modelling nonperturbative frequency sweeping *Proc. 9th IAEA Technical Meeting on Energetic Particles in Magnetic Confinement Systems (Takayama, Japan, 2006)* NIFS-PROC-63
[36] Candy J, Berk H L, Breizman B N and Porcelli F 1999 *Phys. Plasmas* **6** 1822
[37] Todo Y, Shinohara K, Takechi M and Ishikawa M 2005 *Phys. Plasmas* **12** 012503
[38] Fu G Y *et al* 2006 *Phys. Plasmas* **13** 052517
[39] Zonca F, Briguglio S, Chen L, Fogaccia G and Vlad G 2005 *Nucl. Fusion* **45** 477
[40] Gorelenkov N N *et al* 2004 *Phys. Plasmas* **11** 2586
[41] Fredrickson E D *et al* 2003 *Phys. Plasmas* **10** 2852
[42] Heidbrink W W *et al* 2003 *Plasma Phys. Control. Fusion* **45** 983
[43] Fredrickson E D *et al* 2001 *Phys. Rev. Lett.* **87** 145001
[44] Fredrickson E D, Gorelenkov N N and Menard J 2004 *Phys. Plasmas* **11** 3653
[45] Fredrickson E D *et al* 2006 *Phys. Plasmas* **13** 056109
[46] Fredrickson E D *et al* 2002 *Phys. Plasmas* **9** 2069
[47] Ono M *et al* 2000 *Nucl. Fusion* **40** 557
[48] Leblanc B P *et al* 2003 *Rev. Sci. Instrum.* **74** 1659
[49] Budny R V 1994 *Nucl. Fusion* **34** 1247
[50] Lao L L, ST John H, Stambaugh R D, Kellman A G and Pfeiffer W P 1985 *Nucl. Fusion* **25** 1611
[51] Rosenberg A L *et al* 2004 *Phys. Plasmas* **11** 2441
[52] Biewer T M *et al* 2005 *Phys. Plasmas* **12** 056108
[53] Medley S S and Roquemore A L 1998 *Rev. Sci. Instrum.* **69** 2651

[54] Harvey R W and Mccoy M G *Proc. IAEA Technical Committee Meeting on Advances in Simulation and Modeling of Thermonuclear Plasmas (Montreal, Canada, 1992)* (Vienna: IAEA)
[55] Fredrickson E D *et al* 2006 *Nucl. Fusion* **46** at press
[56] Fredrickson E, Chen L and White R 2003 *Nucl. Fusion* **43** 1258
[57] Strachan J D *et al* 1985 *Nucl. Fusion* **25** 863
[58] Gorelenkov N N, Chen Y, White R B and Berk H L 1999 *Phys. Plasmas* **6** 629
[59] Chen L, Vaclavik J and Hammett G W 1988 *Nucl. Fusion* **28** 389
[60] Chu M S, Greene J M, Lao L L, Turnbull A D and Chance M S 1992 *Phys. Fluids* B **4** 3713